Trapping of oxygen vacancies in the twin walls of perovskite

Liliana Goncalves-Ferreira,[1] Simon A. T. Redfern,[1] Emilio Artacho,[1,2] Ekhard Salje,[1] and William T. Lee[3]
[1]*Department of Earth Sciences, University of Cambridge, Downing Street, Cambridge CB2 3EQ, United Kingdom*
[2]*Donostia International Physics Centre, Universidad del Pais Vasco, 20080 San Sebastian, Spain*
[3]*Department of Mathematics and Statistics, University of Limerick, Limerick, Ireland*
(Received 9 September 2009; revised manuscript received 17 December 2009; published 20 January 2010)

The binding and pairwise interaction of oxygen vacancies in the ferroelastic (100) twin walls of the orthorhombic phase of $CaTiO_3$ perovskite (*Pbnm*) have been investigated by numerical simulations using empirical force fields. An oxygen vacancy finds it energetically favorable to reside inside a twin wall, particularly when bridging two titanium ions located in the twin-wall plane. In such case, the binding energy of the vacancy to the wall is 0.7 ± 0.1 eV, the error bar reflecting variability within two different force fields. A different disposition of the vacancy in the wall sees its binding energy reduced by a factor of 2. This implies that depending on the relative time scales for twin-wall motion and for oxygen-vacancy diffusion, anelastic motion of twin walls can display two different energy dissipation mechanisms associated to these point defects. The strongest interactions among oxygen vacancies in a twin wall are due to short-range repulsion so that no defect clusters were found. The vacancy-wall binding energy is found to increase substantially with pressure.

DOI: 10.1103/PhysRevB.81.024109 PACS number(s): 61.50.Ks, 61.72.jd, 61.72.Mm

I. INTRODUCTION

Perovskites have been of longstanding scientific interest in the physics and chemistry of materials, both natural and manmade,[1] the latter ranging from multiferroics to superconductors. The mineral perovskite, $CaTiO_3$, consists of corner linked TiO_6 octahedra with Ca atoms distributed between the octahedra. Its distortion from the ideal cubic structure[2,3] is explained by the tilting of deformable TiO_6 octahedra around their three symmetry axes [Figs. 1(a) and 1(b)]. Under ambient conditions, $CaTiO_3$ exhibits *Pbnm* symmetry and a Glazer octahedral tilt system[4,5] of $a^-a^-c^+$. This structure is analogous to that of the $MgSiO_3$ perovskite, the most abundant solid material in earth, as main component of its lower mantle.

The symmetry reduction from cubic to orthorhombic allows for twinning, which gives rise to twin domains separated by twin walls. These walls can move under mechanical stress.[6,7] This motion and whatever interferes with it (pinning by other defects) is crucial in the understanding of ferroelastic hysteresis, fatigue, and also in dissipation effects in elastic materials response (e.g., in seismic wave attenuation). A simple ferroelastic twin wall [Fig. 1(c)] is described in terms of the relevant (primary) order parameter,[8] Q_1, which is nonzero in the bulk of the twins (it would be zero at the high-symmetry phase), and goes to zero at twin walls while changing sign between twins. In this case Q_1 can be associated with an octahedral tilt. It couples to secondary order parameters, e.g., to other rotational degrees of freedom, ferroelectriclike offcenterings,[9] or octahedral deformations. Secondary order parameters appear or are enhanced in the walls[10] while being suppressed in the bulk, a behavior that can be described within Landau theory by a coupling term of the type $\lambda Q_1^2 Q_2^2$, where Q_2 is the secondary order parameter and $\lambda(>0)$ is the coupling constant (other couplings are possible but depend on the symmetries of the system and the order parameters). This scenario is the main characteristic of so-called chiral walls.[11] Such walls are usually rather wide and not prone to Peierls pinning[12] while their dynamics is still subject to extrinsic pinning by defects.

Experimentally, the accumulation of defects is seen as resonances of wall movements under external stress fields.[13,14] The dynamics of ferroelastic twin walls has been widely studied experimentally[13,15–20] and theoretically,[12,21,22] yet very few papers identify oxygen vacancies as pinning centers and investigate the dynamics of the pinning/unpinning process.[10,14,23–25] Here, we report a detailed inves-

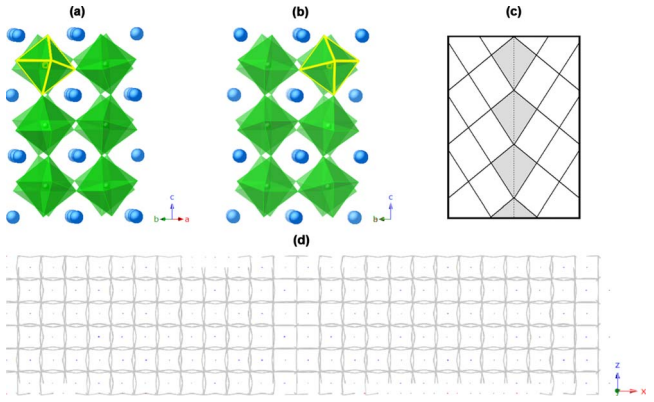

FIG. 1. (Color online) $CaTiO_3$ orthorhombic perovskite showing the tilting of the TiO_6 octahedra at room conditions (a) before and (b) after a 90° rotation along the *c* axis. (c) A common unrelaxed twin wall (gray area) between two ferroelastic domains, oriented along the (110) plane of the tetragonal phase (low-symmetry phase), where the unit cell is represented by rectangles with *a* and *b* parameters (*c* is pointing into the paper) with respect to the cubic phase (Ref. 8). (d) A wire frame view along the *y* axis of the relaxed configuration of the orthorhombic $CaTiO_3$ perovskite structure. Titanium ions reside at the vertices of the sticks and they are bridged by oxygen ions. The (isolated) points are Ca ions. Note the periodicity and the perfect alignment of Ti ions (nontilted octahedra) represented by two straight lines, at the center and at the right corner of the diagram, indicating the actual twin walls locations. The walls are separated by 49.8 Å.

TABLE I. Empirical force fields for $CaTiO_3$ employed in this work: interatomic potentials, structural parameters, tilt angles, and elastic moduli. Model 1 (M1) was derived by Calleja *et al.* (Ref. 25) and M2 was obtained in this work.

Parameter	Experiment	M1	M2
Ca-O: A_{ij} (eV)		2272.741	409.509
Ca-O: B_{ij} (Å^{-1})		3.3490	2.4783
Ca-O: C_{ij} (eV Å^6)		0.00	0.00
Ti-O: A_{ij} (eV)		3242.124	718.661
Ti-O: B_{ij} (Å^{-1})		3.4626	2.4534
Ti-O: C_{ij} (eV Å^6)		0.00	0.00
O-O: A_{ij} (eV)		22764.000	18737792.107
O-O: B_{ij} (Å^{-1})		6.7114	7.8616
O-O: C_{ij} (eV Å^6)		27.88	235.59
a (Å)	5.381[a]	5.389 (+0.1%)	5.298 (−2%)
b (Å)	5.442[a]	5.433 (−0.2%)	5.339 (−2%)
c (Å)	7.641[a]	7.652 (+0.2%)	7.531 (−1%)
V (Å^3)	223.8[a]	224.0 (+0.1%)	213.0 (−5%)
$\alpha=\beta=\gamma$ (deg)	90[e]	90[e]	90[e]
θ_x (deg)	9.3[a]	8.4 (−10%)	9.5 (+2%)
θ_y (deg)	9.4[a]	8.5 (−10%)	9.6 (+2%)
θ_z (deg)	8.8[a]	8.1 (−8%)	8.8 (0%)
K (GPa)	170.9 ± 1.4 [b]	278.4 (+63%)	174.4 (+2%)
μ (GPa)	106.0 ± 1 [c]	164.1 (+55%)	106.0 (0%)
C_{11} (GPa)	308[d]	494 (+60%)	332 (+8%)
$C_{12}=C_{21}$ (GPa)	95[d]	194 (+104%)	97 (+2%)
$C_{13}=C_{31}$ (GPa)	110[d]	153 (+39%)	110 (0%)
C_{22} (GPa)		484	312
$C_{23}=C_{32}$ (GPa)		156	105
C_{33} (GPa)	305[d]	523 (+72%)	303 (−0.7%)
C_{44} (GPa)	110[d]	154 (+40%)	106 (−4%)
C_{55} (GPa)		152	113
C_{66} (GPa)	121[d]	187 (+55%)	100 (−17%)

[a]Experimental structural parameters from Ref. 34.
[b]Experimental bulk modulus K, Ref. 30.
[c]Experimental shear modulus μ, Ref. 35.
[d]Experimental elastic constants (Refs. 31 and 32).
[e]These parameters remained fixed. M2 also included the fitting against 49 phonon frequencies extracted from Ref. 33 (not shown).

tigation of oxygen vacancies in twin walls, their mutual interaction, and influence of pressure on the defect energy.

II. COMPUTATIONAL METHOD

We used two different sets of empirical potentials (Table I) to describe the interactions in $CaTiO_3$. Both models are based on electrostatic interactions of Coulombic type with formal charges on ions and Buckingham potentials between nearest neighbors. These are pair-body potentials describing the rigidity of the TiO_6 octahedra. A cutoff distance of 10 Å was used for nonelectrostatic interactions in both models.

Energy differences were analyzed between relaxed geometries at different conditions of pressure. Small relaxations were performed using GULP (Refs. 26 and 27); the DLPOLY program[28] was used for the relaxation of large simulation cells. It is not trivial to obtain subelectron volt energy differences of relaxed structures when dealing with many thousands of atoms. We used molecular-dynamics (MD) annealing toward zero temperature. Lattice energies obtained by the two models are within 6% of each other and the difference in relevant (small) energies obtained with both codes are within 1%.

An original force-field model was derived by Calleja *et al.*[25] (M1), targeting mostly structural stability properties, and has been used for further applications.[29] The elastic properties were less well determined in this model so that a new parameter set (M2) was fitted here as an extension of M1 by including elastic moduli[30–32] and phonon frequency modes[33] for the fit. The reliability of these models was first tested with small relaxations of variable unit cells (20 atoms), which were performed using static calculations with GULP. Numerical simulations were then extended to a medium-sized system with a supercell of $4\times4\times3$ unit cells (960 atoms), where a mild thermal treatment under variable cell conditions allowed us to confirm the stability of the *Pbnm* phase versus other possible competing phases the model might have wanted to relax onto. These two force fields, quite different, but reasonably describing the material at hand, are used to ascertain the model dependence of the results and conclusion of this paper.

The experimentally observed orthorhombic structure was reproduced by M1 within a maximum error of 0.2% for the unit cell parameters, 4% for all the atomic displacements (x,y,z) in the symmetric unit cell and tilt angles within 1°. M2 reproduces the orthorhombic unit cell parameters within an error of 2%, the atomic positions within 6% and tilt angles within 1°, while the elastic moduli are vastly improved over M1 (see Table I). Details of the octahedral tilting calculation along the three main directions: [100], [010], and [001] (hereafter called x, y, and z, respectively) are in agreement with the experimental values obtained by Sasaki *et al.*[36] and Buttner and Maslen.[37]

Two (100) twin walls were introduced in a supercell of $26\times10\times6$ unit cells [Fig. 1(d)], as in Ref. 9. This configuration needed to be long along the x direction to allow enough separation between the walls but also along y and z to allow for point-defect separation. The simulation cell comprised 7800 atoms with orthorhombic periodic boundary conditions (PBC). Two walls were considered for compatibility with PBC.

The relaxation was originally performed with a cell variable in shape and size (NσT ensemble). This was done by equilibrating in a constant-stress tensor and isothermal environment using a two-stage approach. First, raising the kinetic temperature to 10 K for the first 0.5 ps within MD by scaling all the velocities up. Second, quenching slowly to 0 K until all velocities reach zero and the system had completely relaxed (within 0.1 eV for the final total energy). These simulations used a time step of 1 fs and normally 10 ps of MD were enough to find the minimum. Similarly, the configuration containing the walls and the point defects was further relaxed for variable cell size but fixed cell shape (NPT).

The energies associated with the presence of single point defects (oxygen vacancies) were compared at various loca-

tions and dispositions (between Ti nearest neighbors along x, y, and z) in the neighborhood of the walls, starting from the central twin wall and moving perpendicularly away toward the bulk region (along the x axis of our simulation cell). The first vacancy was selected over the central twin wall of the configuration showed in Fig. 1(d) (taken as reference); and another two, one very close to the former, and finally one very far from the wall.

The introduction of an oxygen vacancy generates a charge imbalance, intractable within PBC. To restore the charge balance, the individual elemental charges in the system were compensated by slightly adjusting the charge of the Ca and Ti ions (without removing any other atom from the configuration). This implies a charge in $\delta q \sim -6.4 \times 10^{-4} e$ over all cations, equivalent to a homogeneous charge background. An explicit counterdopant could have been included instead but that would have introduced additional and unnecessary complexity.

To establish the reliability of our models for our oxygen-vacancy study what matters is not how well a vacancy is described by our potentials but rather how well described is the change in energy when taking the vacancy from the bulk to the twin wall. The difference between the bulk and the twin wall is a small change in tilt angle. Its effect on the vacancy is mostly due to the slight change in electrostatics and strain, both well captured by our models. A good test of this is given by the local relaxations around a vacancy in the bulk of the material. The characteristic feature is the outward relaxation of the two Ti atoms neighboring the vacancy. First-principles calculations of oxygen vacancies in bulk orthorhombic $CaTiO_3$ (see Ref. 38 for a detailed density-functional study of the vacancies, and Ref. 39 for a careful theoretical study of the bulk) give a Ti-vacancy distance of 2.13 Å, when the corresponding bulk Ti-O distance was 1.96 Å. Our respective numbers are 2.11 and 1.95 Å, displaying the same effect in quite quantitative agreement. Furthermore, the mentioned first-principles work[38] also offers equivalent numbers for the cubic phase, namely, 2.03 and 1.94 Å. The twin wall can be considered an environment midway toward the cubic environment (one tilt order parameter vanishes, the others do not). Our numbers for the vacancy at the wall are 2.06 and 1.93 Å, clearly moving toward the bulk cubic values. These agreements for the vacancy and the way it varies toward the wall-like environment give reasonable validation of our models toward the conclusions of this study. First-principles studies for this problem would be desirable but are still out of reasonable reach not because of the size of the system but because of the very long and subtle relaxations.

III. RESULTS

A. Twin-wall structure in $CaTiO_3$ perovskite

The structure of the twin walls is described in terms of order parameters along each of the three crystallographic directions (x, y, and z), which are related to the tilting or rotations of the octahedra around each of the axes. There are two possible tilts for orthorhombic perovskites, which correspond to two order parameters (each of them can be either positive or negative). These order parameters vary with the distance perpendicular to the twin walls and have a shear strain associated with them.

Given the Ti-O and Ti-Ti bond distances, the tilting of the octahedra along each of the crystallographic axes was determined for the relaxed configuration with each of the models. The net tilting of an octahedron is given by

$$\theta = \arccos\left(\frac{r_{\text{Ti-Ti}}}{2r_{\text{Ti-O}}}\right), \tag{1}$$

where $r_{\text{Ti-O}}$ is the Ti-O bond distance for each octahedron and $r_{\text{Ti-Ti}}$ represents the distance between Ti atoms in neighboring octahedra. We will use, however, a Cartesian decomposition of the tilts, adequate for small tilts. They depend on the vector $\vec{d}=\vec{r}_{\text{O}}-\vec{r}_{\text{Ti}}$, between a Ti ion and each of the closest O neighbors that belong to the same octahedron. There are six such vectors per octahedron corresponding to each of the bridging oxygens (two along x, y, and z). Taking the relevant vector in each case, the octahedral tilting along each direction can be described as

$$\theta_x = \arctan\left(\frac{d_z}{d_y}\right),$$

$$\theta_y = \arctan\left(\frac{d_z}{d_x}\right),$$

$$\theta_z = \arctan\left(\frac{d_x}{d_y}\right). \tag{2}$$

Figure 2 displays the behavior of the three tilts as a function of the distance from the central twin wall. They are plotted as the average, the error bars representing the standard deviation, of the different values obtained in the different octahedra in each plane (due to incomplete relaxation and to inequivalent octahedra in the orthorhombic unit cell).

The primary order parameter Q_1 is associated with the octahedral rotation around the y axis, θ_y [Fig. 2(a)]. Q_1 follows closely the hyperbolic tangent

$$\theta_y = \theta_y^0 \tanh[(x-x')/w] \tag{3}$$

corresponding to the functional form expected from Landau theory,[8] where $2w$ is the wall width. The twin angle in the xy plane is approximately 0.5°. θ_x and θ_z show breather anomalies across the wall [Figs. 2(b) and 2(c)], which is the typical behavior expected for secondary order parameters.[10,12] The secondary order parameter Q_2 is represented by a hyperbolic secant profile

$$\theta_x = \theta_x^0 + \text{sech}[(x-x')/w],$$

$$\theta_z = \theta_z^0 + \text{sech}[(x-x')/w]. \tag{4}$$

The octahedral tilt angle in the bulk (θ_y^0) is 8.3° in M1 and 9.5° in M2. For the secondary order parameters along x, the bulk value for the octahedral tilt angle θ_x^0 is 8.3° for M1 and 9.2° for M2. Along z the octahedral tilt angle θ_z^0 is 8.1° for M1 and 8.7° for M2. The bulk octahedral tilt angles for each of the directions, estimated with M2 are always larger than

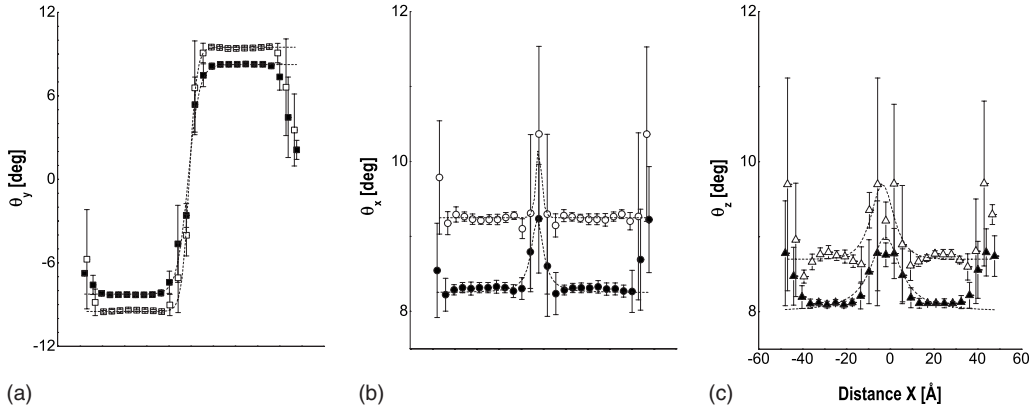

FIG. 2. Octahedral tilting around each of the crystallographic directions: (a) along [010], (b) along [100], and (c) along [001]. Open symbols represent our potential model (M2) and closed symbols correspond to M1 (Ref. 25).

the values obtained with M1, while the relative magnitudes are similar for both models.

The twin-wall width $2w$ for Q_1 was determined for M1 and M2 as 1.09 and 0.84 nm, respectively, which lies well within existing experimental values.[13,40,41] The secondary order parameter along x displays widths of 0.45 and 0.20 nm for M1 and M2, respectively. This result is in agreement with the finding that there is a width difference between primary and secondary order parameters, as discussed by Houchmandzadeh *et al.*,[11] generating larger lattice distortions in the domains than in the walls. However, the secondary order parameter along z shows wall widths closer to the primary order parameter. These values are 1.12 and 0.91 nm, respectively.

An analysis of the geometry around the walls was also performed by measuring the average $r_{\text{Ti-Ti}}$ distances for nearest neighbors perpendicular to the wall, for both M1 and M2 (Fig. 3). These distances increase by $<0.6\%$ and 0.4% at the wall for each of the models, due to the straightening of the Ti-O-Ti bonds. The central wall is located at the position $x=-0.19$ nm, as indicated by the dotted line in Fig. 3.

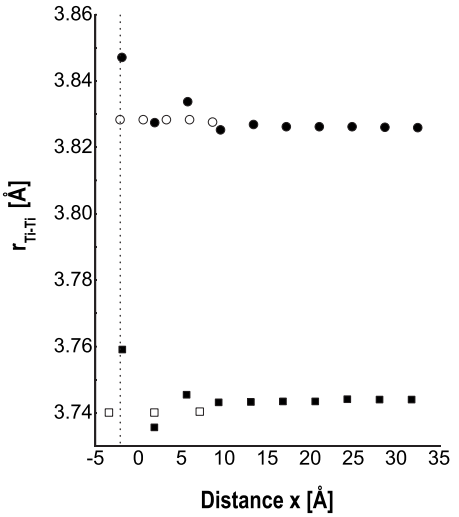

FIG. 3. Ti-Ti nearest-neighbors distances perpendicular to the walls. Open symbols show the distances without twin walls and closed symbols, the distances due to the presence of the walls. Circles are for M1 and squares for M2.

The influence of pressure was initially investigated on the defect-free $CaTiO_3$ perovskite configuration with the (100) ferroelastic twin walls for pressures up to 10 GPa (Table II). The octahedral tilting showed a slight increment along each direction and a small decrease in the wall thickness with increasing pressure. This is as expected, given the fact that the relevant phase transition (for which Q_1 would go to zero) increases its transition temperature with growing P. This wall thinning with pressure relates to the behavior of the order parameter (octahedral tilting). The response in terms of the compressibility of the wall through the squeezing of the octahedra was described in Ref. 42.

B. Twin wall interactions with oxygen vacancies

After introducing oxygen vacancies, the twin wall thickness was determined for the primary and secondary order parameters. The values obtained were smaller (by about 9%) than those derived from the defect-free configuration, which means that the vacancies tend to decrease the thickness of the wall locally. This change in wall width is attributed to the interaction between the primary order parameter and the point defect.[14] The presence of oxygen vacancies at the given concentration of 1.1×10^{-3} vac/Å^2 already has a sizeable effect on the twin walls.

The energies associated with the presence of oxygen vacancies at various locations along [100] were calculated. The vacancy-wall binding energy was computed from the differ-

TABLE II. Wall thickness versus pressure for the (100) ferroelastic wall in $CaTiO_3$.

P (GPa)	$2w$ (nm)
0	1.00 ± 0.02
2	0.95 ± 0.04
4	0.93 ± 0.09
6	0.90 ± 0.06
8	0.89 ± 0.05
10	0.87 ± 0.04

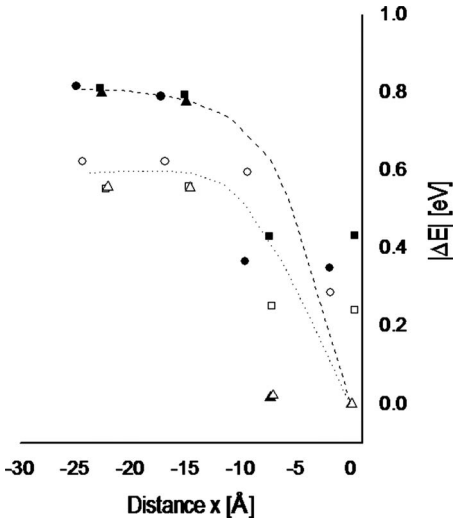

FIG. 4. Relative energies of oxygen vacancies in $CaTiO_3$ with the distance perpendicular to the walls ($P=0$ GPa). Open symbols (and the short dotted line) are for M2 and closed symbols (and the dashed line) are for M1. Circles denote oxygen vacancies bridging titania along [100], squares those bridging along [010] and triangles those bridging along [001].

ence in lattice energy of having a vacancy at the wall and having it midway between walls. It is calculated to be 0.80 eV in M1 and 0.58 eV in M2 (Fig. 4). These values are smaller than the 1.20 eV obtained by Calleja *et al.*[25] for the binding of an oxygen vacancy to a (100) composite wall made of a ferroelastic twin wall and an antiphase boundary.

We find a marked anisotropy in the binding energy with the location of the oxygen vacancy. Vacancies that occur along Ti-O-Ti linkages perpendicular to the wall (along [100] in our setup) are half as bound to the wall than those along [010] and [001] bridges. This implies that, from the point of view of anelastic dissipation, oxygen vacancies would behave as two different kinds of pinning sites depending on their orientation with respect to the wall, the most binding configuration representing two thirds of the total vacancy concentration. Such behavior would be expected if the time scale for wall motion (passing a pinning point) were shorter than the one for oxygen diffusion, and thus the wall would deal with vacancies as it finds them. If, on the other hand, those time scales are reversed, oxygen vacancies in unfavorable orientations would be expected to relocate to the favorable configuration, all vacancies thus pinning the walls equally. Such time scales depend on temperature and pressure, allowing to foresee interesting behaviors that deserve further scrutiny.

C. Interactions among oxygen vacancies in a wall

Vacancies in a wall can cluster or disperse depending on the defect-defect binding energy.[23] Seven possible oxygen vacancies interactions have been considered in the y direction along the central domain wall plane (yz plane), as shown in Fig. 5. The supercell's largest width, along the y direction, allows for a good description of oxygen vacancy pairs. Interactions I1, I2, and I3 correspond to second-, fourth-, and sixth-nearest-neighbor interactions, respectively. The remaining interactions (I4, I5, I6, and I7) correspond to first nearest neighbors, either oriented along y, in diagonal over the yz plane of the wall, or out of the plane and close but not directly bonded to each other.

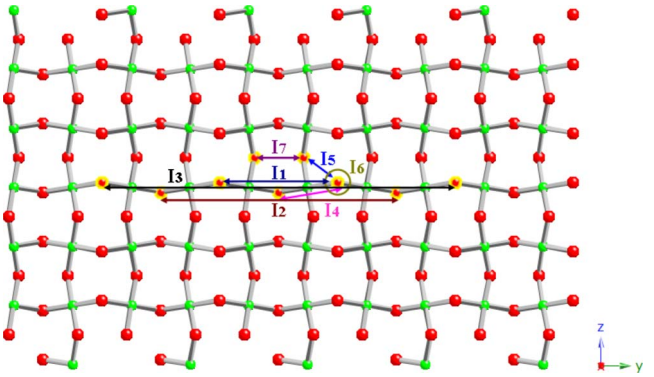

FIG. 5. (Color online) Oxygen vacancy pairs in the plane of the wall.

The corresponding relaxations were performed following the procedure explained in Sec. II, using a NσT ensemble for the two potential models. The interaction energy was determined for each pair of vacancies according to the following equation,

$$E_{int} = E_{pair} + E_0 - 2E_{vac}, \tag{5}$$

where E_{pair} is the potential (lattice) energy for the system with the pair of vacancies, E_0 is the defect-free energy of the system with the two walls, and E_{vac} is the energy associated with each oxygen vacancy system separately. The resulting interaction energies for both potential models are shown in Fig. 6. Both models show an important but quite short-ranged repulsion. The strongest interactions due to short range repulsion are I4 and I5 (between first nearest neighbors). Interaction I1 is very similar to I7 due to the small separation between oxygens on each pair. These results indicate that vacancies are not expected to cluster in domain walls.

D. Pressure dependence of wall pinning

The pressure dependence of twin-wall pinning is of great importance in geophysics where the question is being asked whether anelasticity exists under the high-pressure conditions in the lower mantle. We investigated it as before, the structural optimization being performed under pressures between 0 and 140 GPa, using the NPT ensemble. The pressure effect on the vacancy-wall binding energy is relatively small for both M1 and M2 (Fig. 7), although slightly larger using M2 at intermediate pressures. This reflects the fact that the first model is stiffer than the second. It is clear from both models that the binding energy of an oxygen vacancy increases very slowly at first but becomes substantially enhanced at high pressure. The high-pressure regime seems to start at 80 GPa in model M1 while model M2 shows a steep increase at pressures above 60 GPa. The elastic compressibility of the twin wall is roughly in the same order of mag-

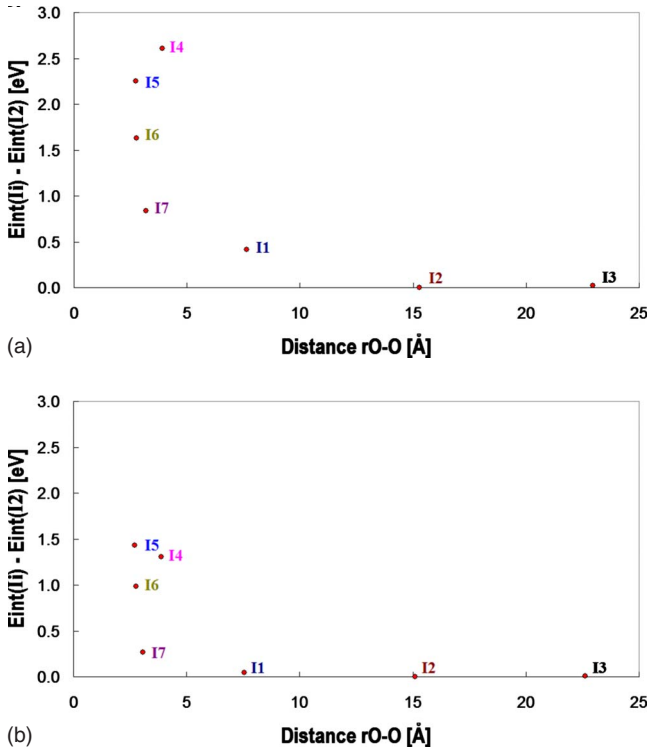

FIG. 6. (Color online) Interaction energy dependence with distance between oxygens for seven different pairs of oxygen vacancies located on the central ferroelastic wall. (a) Results derived from M1 and (b) from M2.

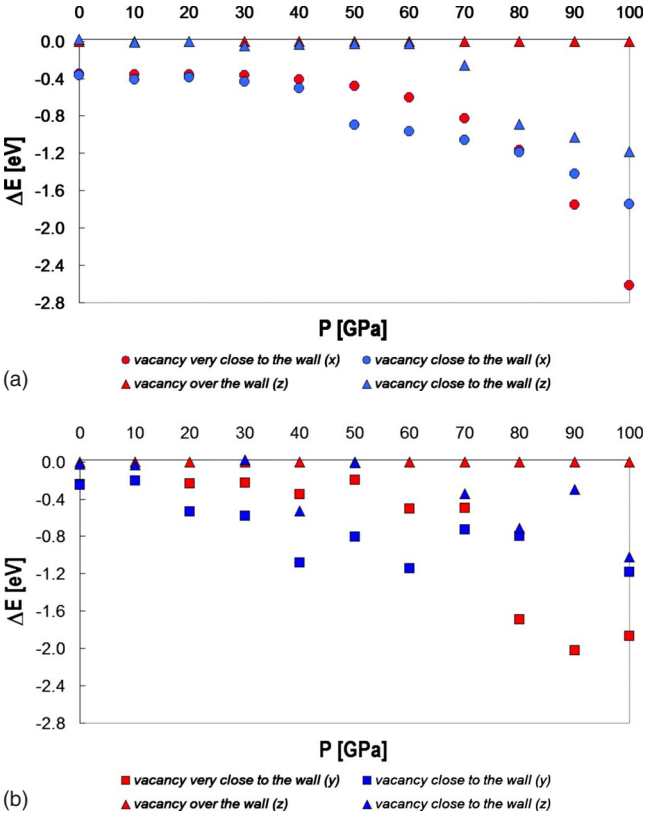

FIG. 7. (Color online) Pressure dependence of the stabilization of oxygen vacancies at the domain wall in $CaTiO_3$ perovskite for: (a) M1 (Ref. 25) and (b) M2, measured relative to the stabilization of a vacancy at the [001] Ti-O-Ti bridge at 0 GPa.

nitude as that of the bulk[42] so that this effect is not related to a simple differential compression of the twin wall. The results imply that twin walls become more efficient sinks for oxygen vacancies as pressure increases, and that oxygen vacancies become stronger pinning defects for walls at high pressure.

IV. CONCLUSIONS

Two force-field models have been used to study the interactions of oxygen vacancies with twin walls in perovskite. First, the twin walls themselves were simulated giving a good description of the behavior of the primary order parameter versus distance to the wall. The secondary order parameters were observed to describe slight breathers at the walls related to octahedral rotations along [100] and [001]. Both behaviors nicely followed the predictions of Landau theory.

Oxygen vacancies were found to bind to the walls more strongly when bridging titanium ions within the wall plane, otherwise their binding energies being reduced by half. The binding energy is calculated to be 0.80 and 0.58 eV for M1 and M2, respectively. Their qualitative agreement supports these conclusions. A dependence on vacancy orientation with respect to the wall has been found that could have interesting implications in the anelastic response of the material depending on the relative time scales of wall motion and vacancy diffusion.

Oxygen vacancies were also found to repel each other when in close proximity in a wall, indicating no clustering of vacancies in walls, although the vacancy-vacancy repulsion was found to decay quite rapidly. The binding of vacancies to walls has been also found to increase with pressure, noticeably so for very high pressures (>80 GPa).

ACKNOWLEDGMENTS

L.G.F. acknowledges support by the U.K.'s NERC and BP through the Dorothy Hodgkin program of the University of Cambridge. W.T.L. acknowledges the support of the Mathematics Applications Consortium for Science and Industry (www.macsi.ul.ie) funded by the Science Foundation Ireland Mathematics Initiative under Grant No. 06/MI/005. The calculations were performed within Cambridge's CamGRID infrastructure.

[1] L. G. Tejuca and J. L. G. Fierro, *Properties and Applications of Perovskite-Type Oxides* 1st ed. (CRC, New York, United States, 1993).
[2] H. P. Rooksby, Nature (London) **155**, 484 (1945).
[3] H. D. Megaw, Proc. Phys. Soc. London **58**, 133 (1946).
[4] A. M. Glazer, Acta Crystallogr., Sect. B: Struct. Crystallogr. Cryst. Chem. **28**, 3384 (1972).
[5] A. M. Glazer, Acta Crystallogr., Sect. A: Cryst. Phys., Diffr., Theor. Gen. Crystallogr. **31**, 756 (1975).
[6] R. J. Harrison, S. A. T. Redfern, and J. Street, Am. Mineral. **88**, 574 (2003).
[7] R. J. Harrison, S. A. T. Redfern, A. Buckley, and E. K. H. Salje, J. Appl. Phys. **95**, 1706 (2004).
[8] E. K. H. Salje, *Phase Transitions in Ferroelastic and Co-Elastic Crystals*, student edition (Cambridge University Press, Cambridge, United Kingdom, 1993).
[9] L. Goncalves-Ferreira, S. A. T. Redfern, E. Artacho, and E. K. H. Salje, Phys. Rev. Lett. **101**, 097602 (2008).
[10] W. T. Lee, E. K. H. Salje, and U. Bismayer, Phase Transitions **76**, 81 (2003).
[11] B. Houchmandzadeh, J. Lajzerowicz, and E. Salje, J. Phys.: Condens. Matter **3**, 5163 (1991).
[12] W. T. Lee, E. K. H. Salje, L. Goncalves-Ferreira, M. Daraktchiev, and U. Bismayer, Phys. Rev. B **73**, 214110 (2006).
[13] R. J. Harrison, S. A. T. Redfern, and E. K. H. Salje, Phys. Rev. B **69**, 144101 (2004).
[14] W. T. Lee, E. K. H. Salje, and U. Bismayer, Phys. Rev. B **72**, 104116 (2005).
[15] J. Sapriel, Phys. Rev. B **12**, 5128 (1975).
[16] T. J. White, R. L. Segall, J. C. Barry, and J. L. Hutchison, Acta Crystallogr., Sect. B: Struct. Sci. **41**, 93 (1985).
[17] D. I. Savytskii, L. O. Vasylechko, M. Berkowski, J. Fink-Finowicki, R. Aleksiyko, P. Byszewski, and A. O. Matkovskii, Ferroelectrics **254**, 121 (2001).
[18] D. Savytskii, A. Senyshyn, A. Matkovskii, L. Vasylechko, K. Wieteska, W. Wierzchowski, T. Lukasiewicz, and U. Bismayer, Z. Kristallogr. **218**, 17 (2003).
[19] D. I. Savytskii, D. M. Trots, L. O. Vasylechko, N. Tamura, and M. Berkowski, J. Appl. Crystallogr. **36**, 1197 (2003).
[20] E. R. Kipkoech, F. Azough, and R. Freer, J. Am. Ceram. Soc. **88**, 768 (2005).
[21] J. Novak and E. K. H. Salje, Eur. Phys. J. B **4**, 279 (1998).
[22] W. T. Lee, E. K. H. Salje, and U. Bismayer, J. Phys.: Condens. Matter **15**, 1353 (2003).
[23] J. H. Harding, Rep. Prog. Phys. **53**, 1403 (1990).
[24] M. S. Islam, Solid State Ionics **154-155**, 75 (2002).
[25] M. Calleja, M. T. Dove, and E. K. H. Salje, J. Phys.: Condens. Matter **15**, 2301 (2003).
[26] J. D. Gale, J. Chem. Soc., Faraday Trans. **93**, 629 (1997).
[27] J. D. Gale and A. L. Rohl, Mol. Simul. **29**, 291 (2003).
[28] W. Smith, T. R. Forester, I. T. Todorov, and M. Leslie, *The DL_POLY_2 user manual, CCLRC Daresbury Laboratory* (Daresbury, Warrington, United Kingdom, 2006).
[29] K. Trachenko, M. Pruneda, E. Artacho, and M. T. Dove, Phys. Rev. B **70**, 134112 (2004).
[30] N. L. Ross and R. J. Angel, Am. Mineral. **84**, 277 (1999).
[31] M. A. Carpenter, P. Sondergeld, B. Li, R. C. Liebermann, J. W. Walsh, J. Schreuer, and T. W. Darling, J. Min. Pet. Sci. **101**, 95 (2006).
[32] M. A. Carpenter, Am. Mineral. **92**, 328 (2007).
[33] E. Cockayne and B. P. Burton, Phys. Rev. B **62**, 3735 (2000).
[34] A. R. Chakhmouradian and R. H. Mitchell, J. Solid State Chem. **138**, 272 (1998).
[35] Y. D. Sinelnikov, G. Chen, and R. C. Liebermann, Phys. Chem. Miner. **25**, 515 (1998).
[36] S. Sasaki, C. T. Prewitt, J. D. Bass, and W. A. Schulze, Acta Crystallogr., Sect. C: Cryst. Struct. Commun. **43**, 1668 (1987).
[37] R. H. Buttner and E. N. Maslen, Acta Crystallogr., Sect. B: Struct. Sci. **B48**, 644 (1992).
[38] H. Lee, T. Mizoguchi, T. Yamamoto, and Y. Ikuhara, Mater. Trans. **50**, 977 (2009).
[39] R. I. Eglitis and D. Vanderbilt, Phys. Rev. B **78**, 155420 (2008).
[40] E. K. H. Salje, S. A. Hayward, and W. T. Lee, Acta Crystallogr., Sect. A: Found. Crystallogr. **61**, 3 (2005).
[41] J. Chrosch and E. K. H. Salje, J. Appl. Phys. **85**, 722 (1999).
[42] L. Goncalves-Ferreira, S. A. T. Redfern, E. Artacho, and E. K. H. Salje, Appl. Phys. Lett. **94**, 081903 (2009).